Off-Axis-NOTE-SIM-23
October 28th 2003

Simulation of a Solid Scintillator Off-axis Detector

Peter Litchfield, Leon Mualem, David Petyt

Introduction

We have made a comprehensive and realistic simulation of the raw data, reconstruction and analysis of a 50 kiloton scintillator/wood detector placed in the NUMI neutrino beam 10km off-axis at 735 km from Fermilab. $\nu_\mu \rightarrow \nu_e$ oscillations at the CHOOZ limit are assumed. The event generation and reconstruction are described. ν_e events are separated from background by a succession of cuts and by a likelihood analysis. Finally a figure of merit (FOM) equal to the number of signal events divided by the square root of the number of background events is calculated and compared with previous analyses.

Scintillator Detector Simulation

Simulation framework

The simulations were done using a version of GMINOS, the GEANT based simulation code used for the MINOS detector. This allows the efficient use of some of the tools that have been developed for implementing and analyzing a scintillator detector. The neutrino interactions were performed by NEUGEN2, which is integrated into the GMINOS code. The output files are ADAMO tables. There were several modifications that were required to correctly implement the new photodector and strip geometry which are described here.

Detector Definition

The GMINOS code is designed to efficiently allow the description of a detector made up of planes of absorber and active detector, with strips oriented along the X or Y axes, and/or at an angle of 45 degrees to these axes. The overall dimensions of the detector, shown in figure 1, are 30m wide, 15m tall, and 162m long. This consists mainly of passive absorber and 900 effective planes of active detector, half with strips oriented along the X axis, and half with strips oriented along the Y axis. The proposed detector is different from MINOS, in that the active detectors are located in 2 layers, made of 150cm wide modules alternating in each layer, with no overlap. Figure 2 shows the layout for the X type plane, with strips oriented along the X axis. The individual modules are 15m

long with the readout ends located along the outer edges. The hatched areas are filled with absorber, and the open areas indicate scintillator modules for the two layers forming a single plane. Figure 3 shows the layout for the planes with strips oriented along the Y axis. The modules are the same size, and are arranged in two different layers as they are in the X planes.

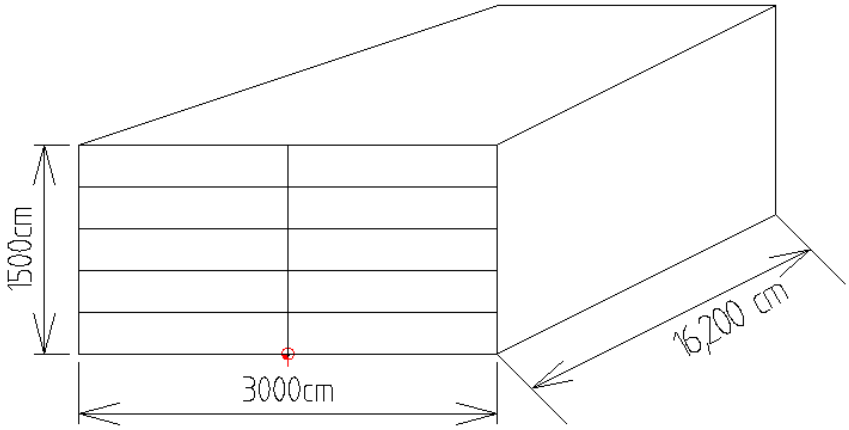

Figure 1 Schematic diagram of the scintillator detector as implemented.

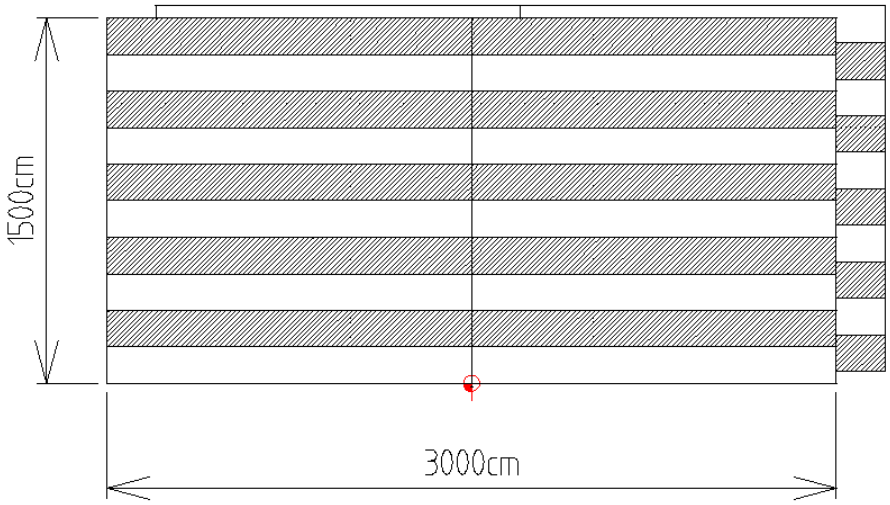

Figure 2 Implementation of modules for X planes, shaded modules are read out in each layer and the unshaded modules are ignored. Each layer is made of 2 15mx15m square sections.

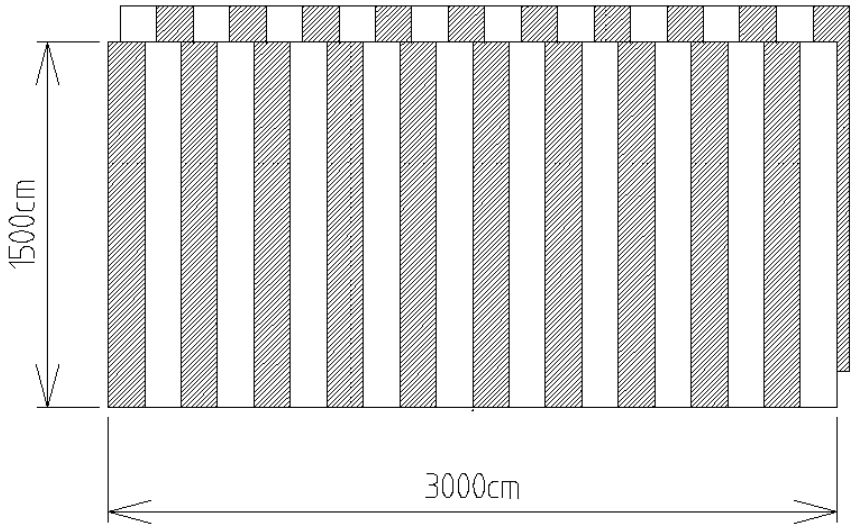

Figure 3 Implementation of modules for the simulated Y axis planes. The shaded modules are read out in each layer, and the unshaded are ignored.

Simulated plane design

The absorber material was implemented as continuous sheets of a low density Lucite. The radiation length of which is very similar to wood, and will be referred to as wood in this document. The density was decreased in GEANT to 0.7g/cc to accurately reproduce the distribution of neutrino interaction vertices. Each active plane plus absorber was 0.36 of a radiation length. The alternating modules in the simulation were implemented as two continuous layers of scintillator modules separated by a one inch layer of wood. The formulation of the alternating modules was done at the analysis stage rather than generation by logically ignoring any hits in half of each layer as indicated in the figures. The Y axis planes are straightforward to implement in the GMINOS framework. The first Y-type plane has an absorber with a thickness of 12.5cm, and an active scintillator plane, and the second Y-type plane has a thin, 2.5cm absorber and an active scintillator plane.

The X axis planes have an additional complication. These planes need to have a cut in the middle so that the readout of the fibers can be done separately for each side. This was done by implementing each 30m by 15m active layer in an X axis plane as two 15m by 15m layers of scintillator. These elements cannot be placed at the same position along the Z direction, so they are placed as close to each other as possible. This has the effect of putting the X axis detectors in the East side of the detectors one scintillator module thickness, 1.05cm further upstream than the modules on the West half of the detector, where they would actually be coplanar in the proposed detector. In addition, since we want the absorber planes to extend the full width of the detector, they are implemented as their own planes with a zero thickness active plane. In a similar way the active planes are implemented as offset scintillator planes with zero thickness absorber. This means that the X planes are actually implemented as 6 X planes. The first plane is a full width 12.5cm thick absorber only plane. The second is a scintillator only plane on the –X half

of the detector. The third plane is an identical scintillator plane shifted to the +X half of the detector. The next 3 planes are the same, except that the absorber is only 2.5cm thick. This makes the numerology of the analysis more complicated since there are 6 X planes and 2 Y planes in a unit cell, but most importantly, it accurately represents the proposed detector.

Scintillator module design

The simulation of scintillator modules themselves was a copy of the MINOS module simulation. The width of all of the modules is 300cm, each containing 75 4cm wide scintillator strips. As discussed above, these are logically cut in half during the analysis and the top 38 or bottom 37 strips of each module are read out from the consecutive layers along the Z axis. The strips themselves are 1cm thick in total with a dead layer of 0.25mm on all sides made of TiO_2 loaded polystyrene, as in the actual strips. The outer skins of the modules were implemented as 0.25mm Iron, to match the proposed material.

Simulation of the readout

The light collection and transmission in the fiber was simulated using the code for the MINOS light collection. The looped fiber was approximated by assuming MINOS style single ended readout with an average of 35 photoelectrons collected at 15m. The attenuation measured for the looped configuration, giving an attenuation length of 404cm falling to a constant level of 21.8% of the un-attenuated level, was used. A wls fiber tail of length 1m and no clear fiber were incorporated. An APD with a quantum efficiency of 85% was assumed. The parameters of the APD gain and noise given in reference 1 were used. The APD output was smeared in accordance with these parameters. The generated pulse height distribution as a function of distance along the strip is shown in Figure 4 and the pulse height distribution as a function of the number of particles crossing the strip in Figure 5.

Event generation

Several types of interactions were simulated, spanning the range of energies, neutrino types and interactions. The neutrino interactions were chosen with a 1/E energy distribution so that the interacted neutrino spectrum is approximately flat in 2 energy ranges, a low energy range from 100MeV to 3GeV, and a high energy range spanning 3GeV to 20GeV. Six data sets were generated, low and high energy, ν_μ CC, ν_e CC and NC. NC events were generated separately because generating them simultaneously in GMINOS produces only 30% as many NC as CC events and the statistics on the NC background suffers. Neutrino and anti-neutrino samples were generated but only the neutrino analysis will be described here. Two samples of events were generated, one as a training sample for the event cuts and one as a test sample. Approximately 230,000 events were generated in each of the six samples for the training sample and 200,000 events for the test sample, a total of approximately 2.5M events.

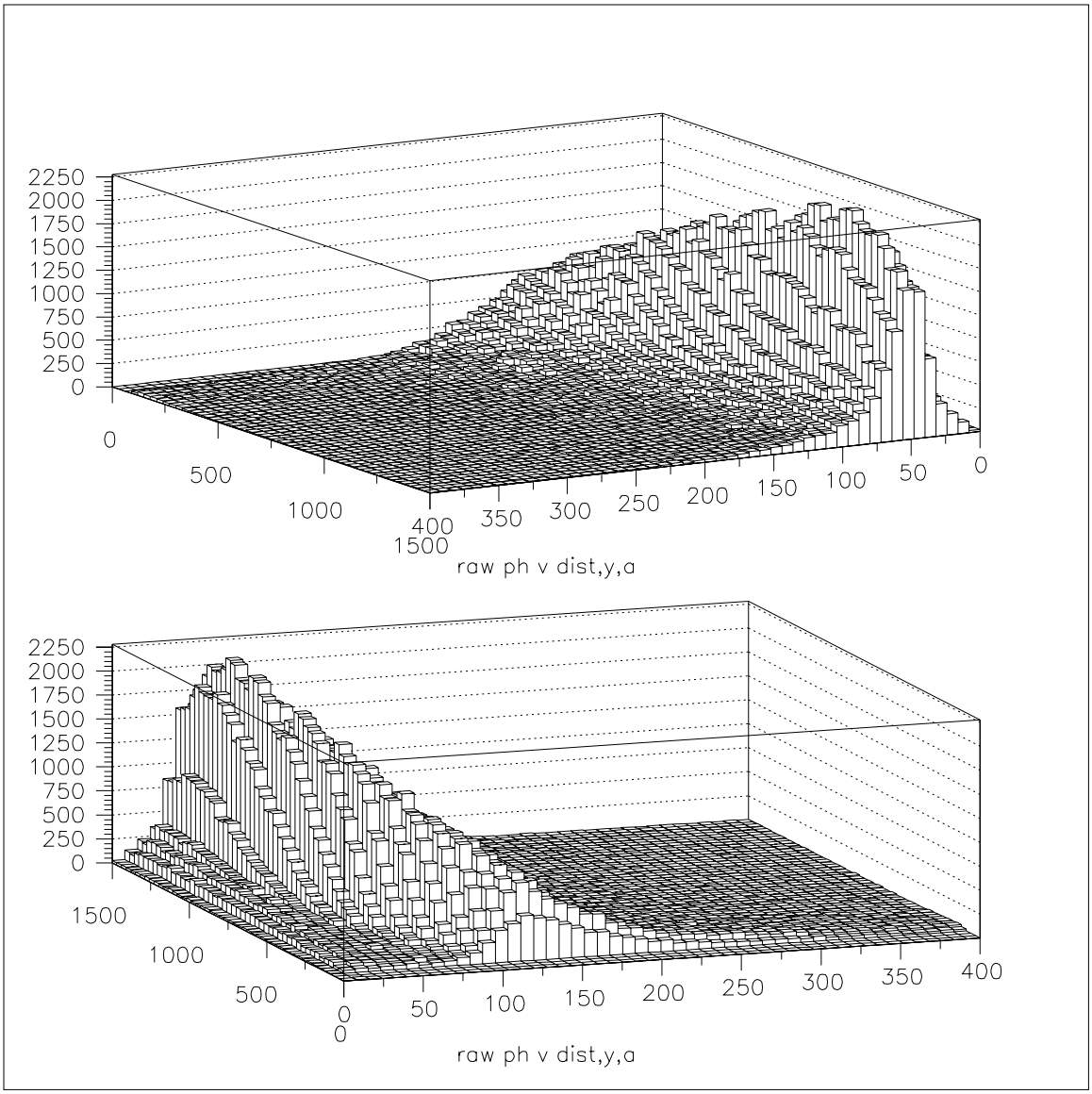

Figure 4: Pulse height as a function of distance along a strip, viewed from the far end (top) and APD end (bottom).

Event Reconstruction

A loose clustering algorithm was applied to the events, which grouped together hits in each view that occur within a distance of 2m of each other. Clusters in the two views were matched by the correspondence of their start and end positions in z (along the beam). The matched cluster with the largest number of hits was selected as the event. The large majority of events only produced one matched cluster. Events with no matched clusters were rejected. In addition the event was required to have a minimum of three hits in each view. The clustering removed outlying hits from events and rejected low energy (chiefly neutral current) events.

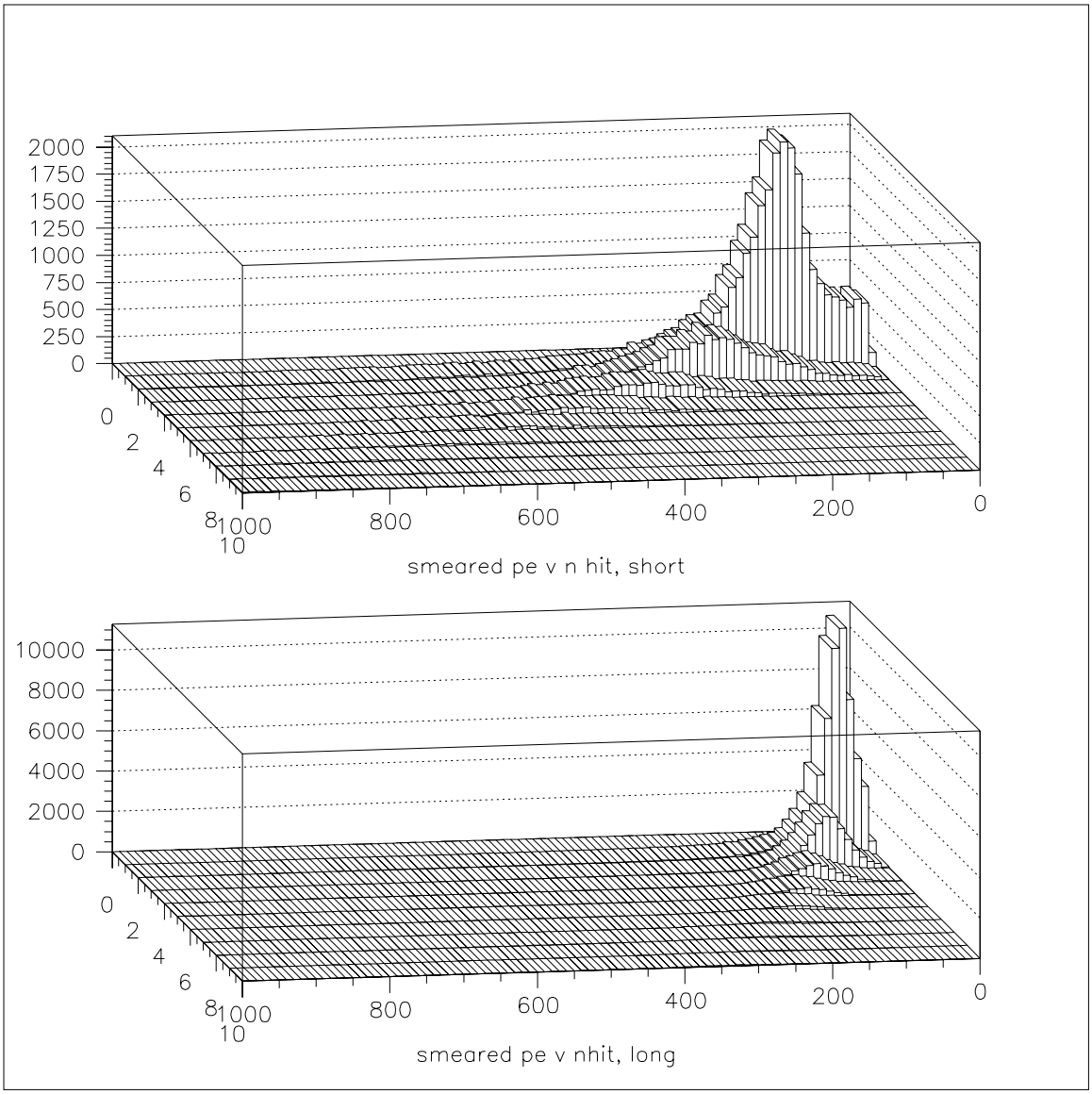

Figure 5: Pulse height distributions as a function of number of particles crossing a strip at the APD end (top) and the far end (bottom).

Events with more than two hits outside the fiducial volume of the detector (50cm in x and y and 2m in z) were rejected at this stage, 86% of reconstructed ν_e events (79% of total events) passed this fiducial requirement.A straight line was fitted to the clusters in each view and the hit and pulse height residuals were calculated. The rms of the hit and pulse height distributions in the beam direction were also calculated. Using the information on the position along the strip given by the fit the measured pulse height was corrected for attenuation

The event cluster was then passed through a filter which used the Hough Transform to select the most significant track-like segment of the event. This filter is an iterative procedure where the 2-dimensional hits (x_i,y_i) in the cluster are transformed into

trajectories in the parameter space (ρ,d) where the relation $x_i\cos\rho+y_i\sin\rho-d=0$ is asserted. The parameters of the most significant track-like segment of the event were taken to be those where the peak in (ρ,d) space occurs, and the hits belonging to the track were those whose trajectories passed within a preset minimum distance to this peak. The procedure was repeated with finer binning in (ρ,d) space and more stringent cuts on the minimum distance to the peak. Figure 6 illustrates the effect of the filter for sample ν_μ CC, NC and ν_e events. In this implementation, electron showers tend to be sufficiently narrow that most of the shower hits were included in the track-like object, whereas fewer hits were tagged as track-like for NC showers, which are generally more diffuse. A straight line was fitted to the hits assigned to the Hough track and again the transverse residual and longitudinal rms in each view calculated.

A set of ntuples was produced which are used in the following analysis to select ν_e events. Copies of the ntuples and/or the GMINOS output files are available.

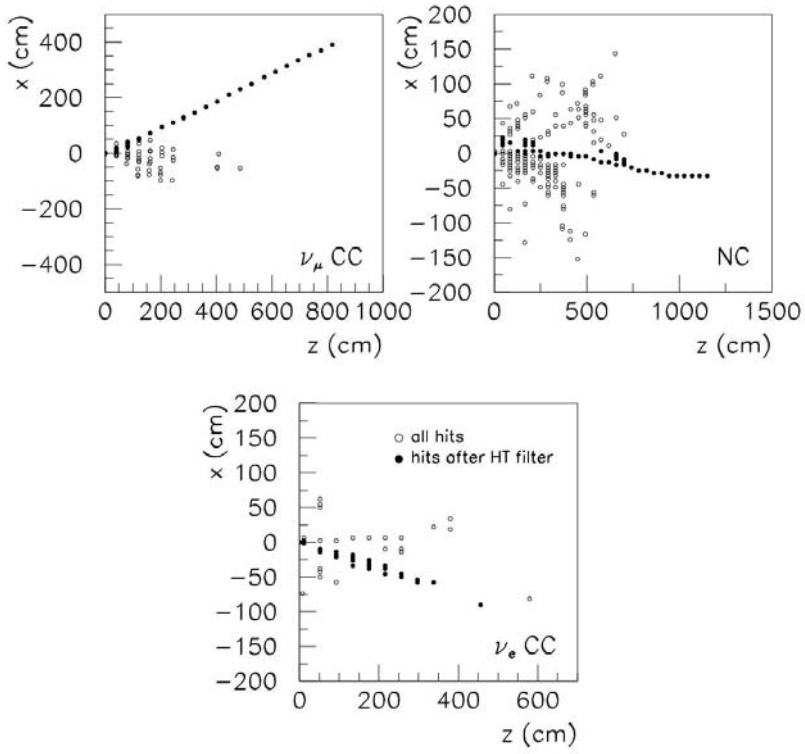

Figure 6 Use of the Hough Transform filter on three example events. The open circles show all the hits in the event and the filled circles show the hits that remain after the filter is applied.

Event weighting

As described above, the events were generated flat in energy. In order to represent the expected event distributions in the detector they were weighted by the following factors;

1. The beam neutrino energy distributions for a location 10km off axis and 735 km from Fermilab as given in the beam file stored on the Fermilab afs /afs/fnal.gov/files/code/off-axis/off-axis_01/beam for this configuration.
2. The oscillation probability, for $\nu_\mu \rightarrow \nu_\mu$ with $\sin^2 2\theta_{23}=1.0$ and $\Delta m^2=2.5\times10^{-3}$ eV^2, and for $\nu_\mu \rightarrow \nu_e$ with $\sin^2 2\theta_{13}=0.1$.
3. A weight for the different density of events in the two generated energy regions and to allow for events lost due to GMINOS crashes.
4. For the NC events a weight for the NC/CC ratio as a function of energy.

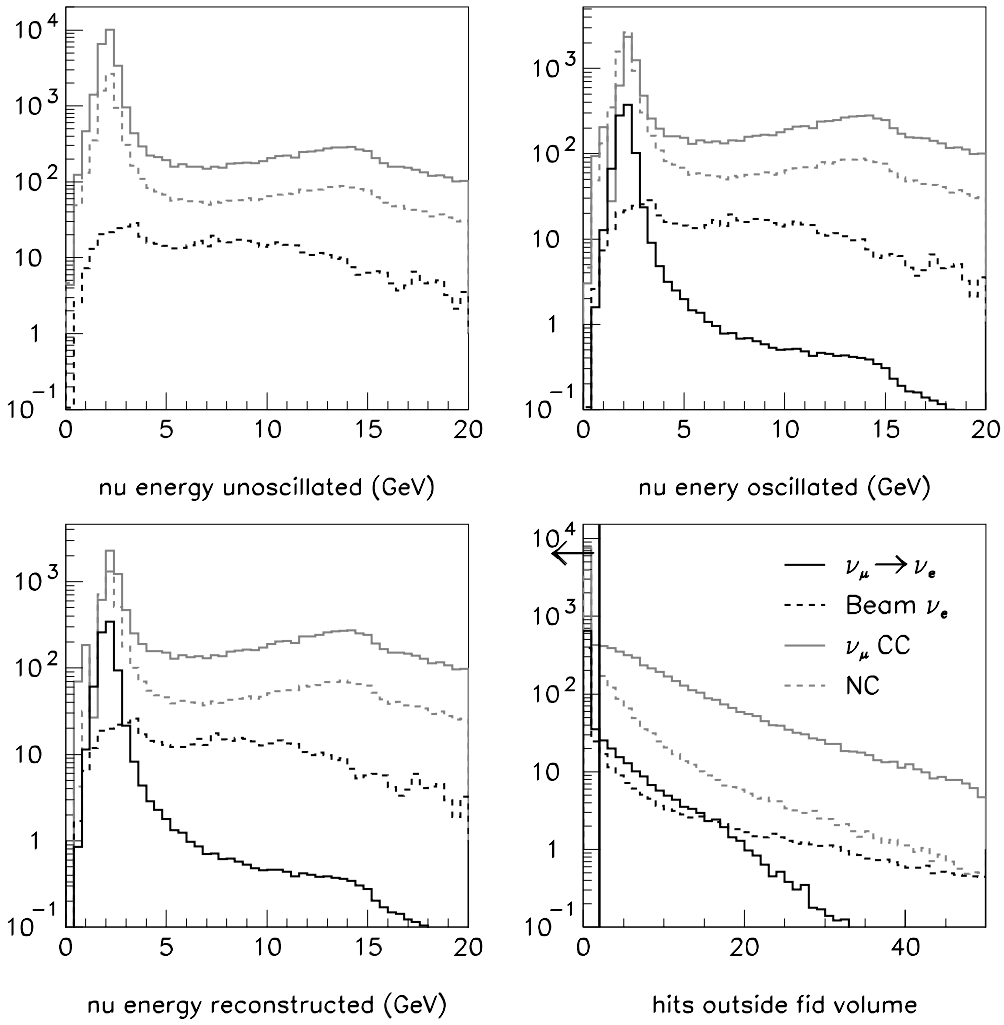

Figure 7 Event samples used in this analysis. Top left: unoscillated true neutrino energy distributions. Top right: energy distributions after oscillations. Bottom left: energy distributions for events that form a valid cluster. Bottom right: distributions of numbers of hits outside the fiducial volume of the detector. Events with more than 2 hits outside the fiducial volume are rejected.

The events were finally normalized to the expected rate of 26898 ν_μ CC events in a 5 year exposure of a 50 kiloton detector. The numbers of events in the four classes, ν_μ CC, NC, ν_e CC from the beam and ν_e CC oscillated from ν_μ are given in Table 1 and shown in Figure 7.

Selection of ν_e CC events

The selection process was in two stages. Firstly a set of cuts was applied which rejected background events with as small as possible effect on the ν_e CC events. The background events remaining after these cuts have a strong overlap with the desired sample. Further separation was obtained by forming a likelihood ratio using a number of variables and cutting on this ratio.

We first show selections using the pulse height information from the scintillator. The initial cuts are applied consecutively on the variables shown in figures 8 and 9 and are:

1. 200 < event length < 700 cm (rejects long muon tracks and short NC events)
2. 8000 <total pulse height < 18000 pe (rejects low-y NC and high energy ν_e CC events)
3. fraction of hits found by Hough Transform > 0.7 (preferentially selects low-y ν_e CC events)
4. hits/plane on the Hough track >1.3 (selects showering events)
5. cosine of the angle between the Hough track and the beam > 0.85 (rejects poorly reconstructed and high-q events)

The weighted number of events remaining after each cut are shown in Table 1.

A likelihood analysis was then performed on the remaining events. One or two dimensional histograms of the variables in the following list were constructed for each of the event types and normalized to a total of 1.0. This then served to define a probability for any given event that it came from any of the samples. A total likelihood for any sample was found by multiplying all of the probabilities. Three log likelihood ratios between the oscillated ν_e hypothesis and the other three hypotheses were formed and plotted. Finally cuts were applied to these ratios to define the final ν_e sample.

The following variables were used in the likelihood analysis;

1. the events remaining after the cuts in the five cut variables
2. the maximum gap (i.e. planes with no hits) in the event
3. the transverse pulse height weighted residual
4. the pulse height in the Hough track
5. total pulse height vs. pulse height weighted transverse residual
6. total pulse height vs. pulse height weighted transverse residual of the Hough track
7. cosine of the angle between the Hough track and the beam vs. total pulse height
8. longitudinal rms of the pulse height vs. total pulse height

The distributions of these quantities are shown in figures 10-15

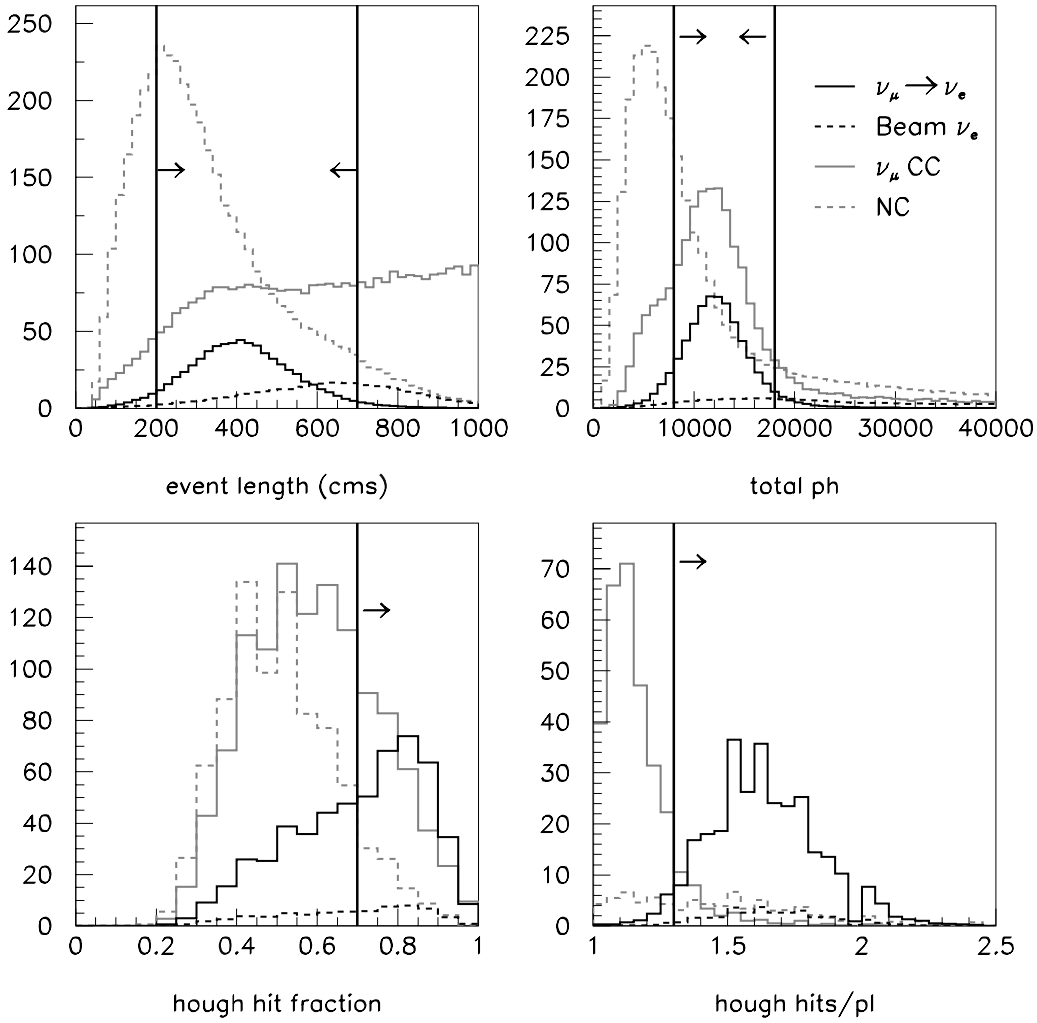

Figure 8 Event distributions used for the cuts. The vertical lines define the cuts, events on the sides towards which the arrows are pointing pass the cuts. The cuts are performed sequentially in the following order. Top left; event length. Top right; summed pulse height. Bottom left; the fraction of hits in the event found by the Hough Transform filter. Bottom right; the number of hits per plane in the Hough track.

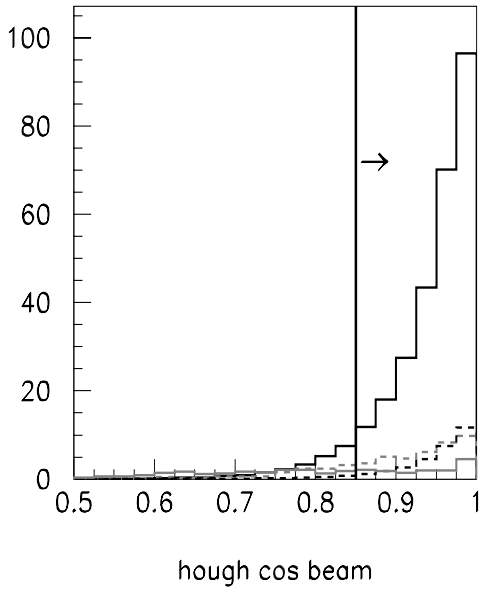

Figure 9 The final cut; the cosine of the angle between the Hough track direction and the z-axis.

Cut	ν_μ CC	NC	beam ν_e	$\nu_\mu \rightarrow \nu_e$ signal
generated events	382386	303224	365750	
Beam weighted	26898.5	7639.9	488.1	
beam weighted +osc	10830.6	7639.9	488.1	778.1
reconstructed events	10501.4	4332.5	442.0	708.8
fiducial volume	7007.8	3755.8	346.9	600.9
event length	1562.7	2438.2	202.6	541.8
total ph	985.4	727.6	55.1	465.0
Hough fraction	256.2	75.9	27.5	255.7
Hough hits/plane	27.9	51.2	26.6	246.4
Hough beam angle	10.9	35.8	24.7	227.5
Likelihood	3.1	12.5	17.5	178.3
Statistical error	0.4	0.9	0.2	1.4
Events remaining	78	407	24144	24144

Table 1 Breakdown of the weighted number of events remaining after the successive cuts. The last row gives the number of unweighted events remaining after all cuts. Note that the generated events totals do not include events that produced no hits in the detector.

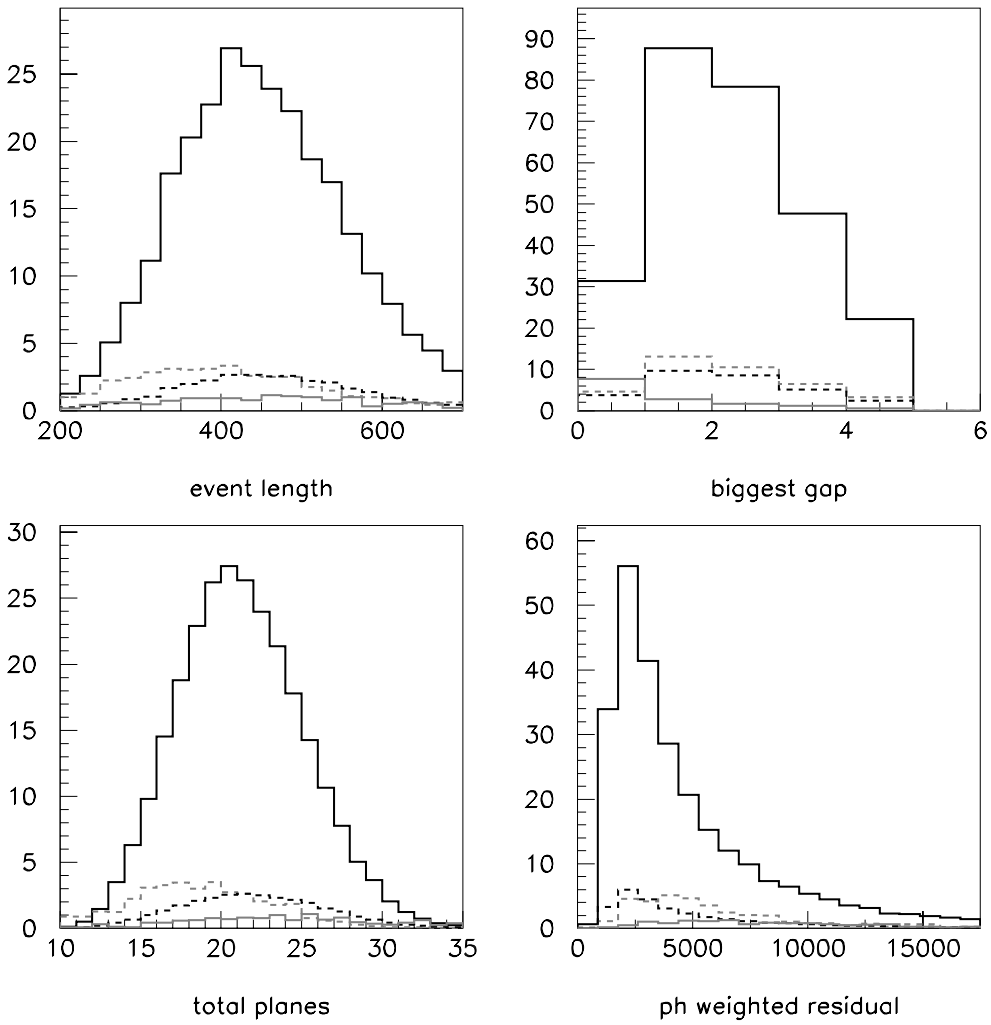

Figure 10 Distributions used in the likelihood function. Top left; the event length after the cuts. Top right; the largest gap (missed planes) in the event. Bottom left; The total number of hit planes in the event. Bottom right; the pulse height weighted residual to the straight line fitted to the event.

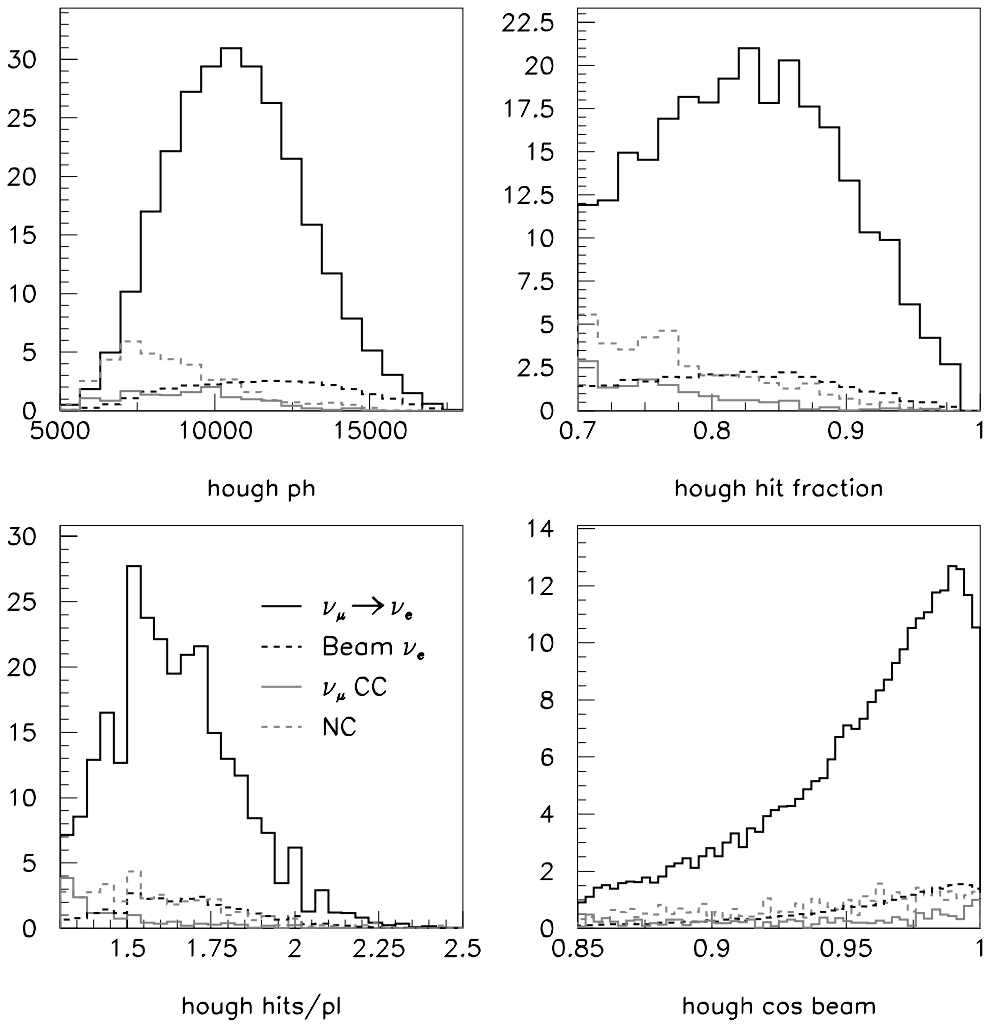

Figure 11 Distributions derived from hits selected by the Hough Transform (HT) filter. Top left: total pulse height. Top right: fraction of hits selected by HT filter over the total number of hits in the event. Bottom left: number of hits per plane. Bottom right: cosine of the angle between the straight line fit to the hits and the z axis.

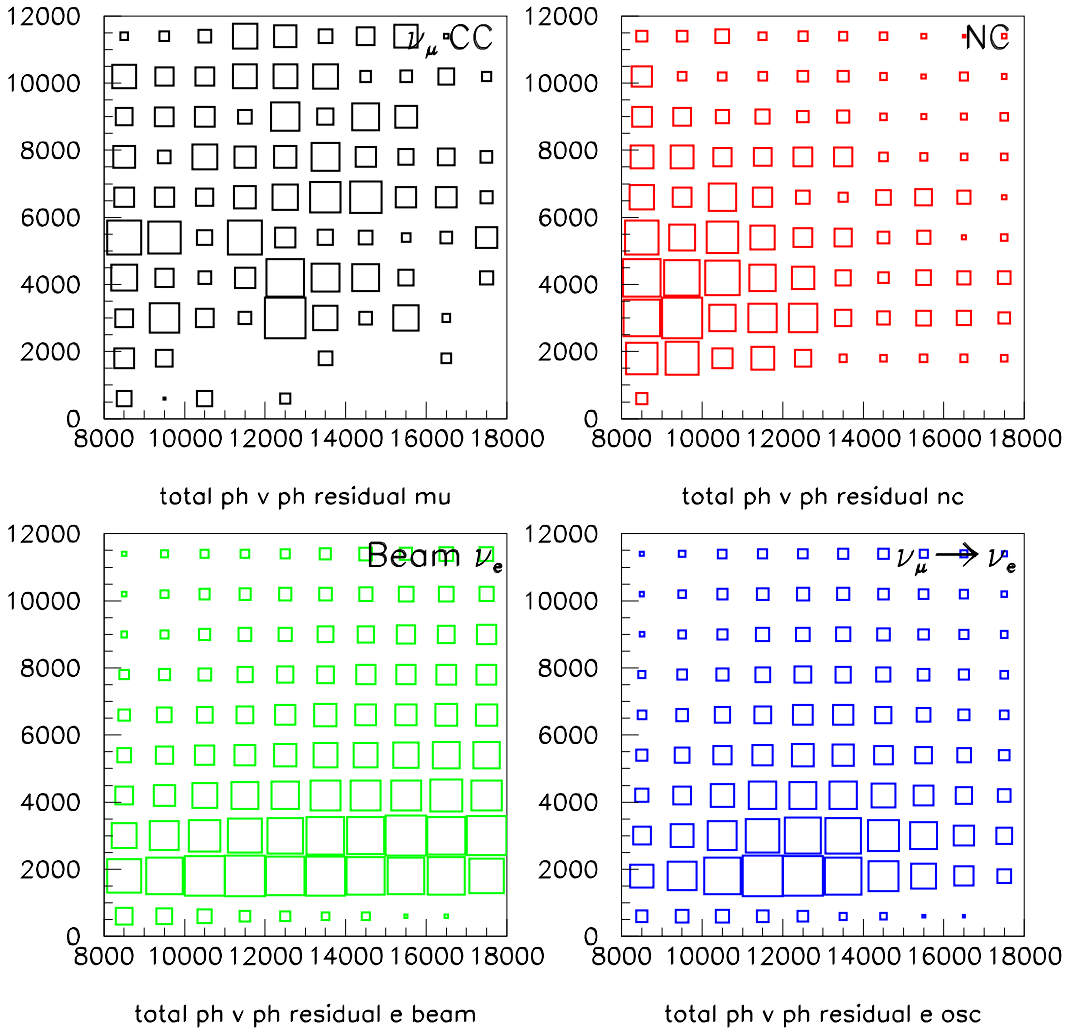

Figure 12 Total pulse height (x) versus pulse height residual (y) distributions for all hits in the four event classes.

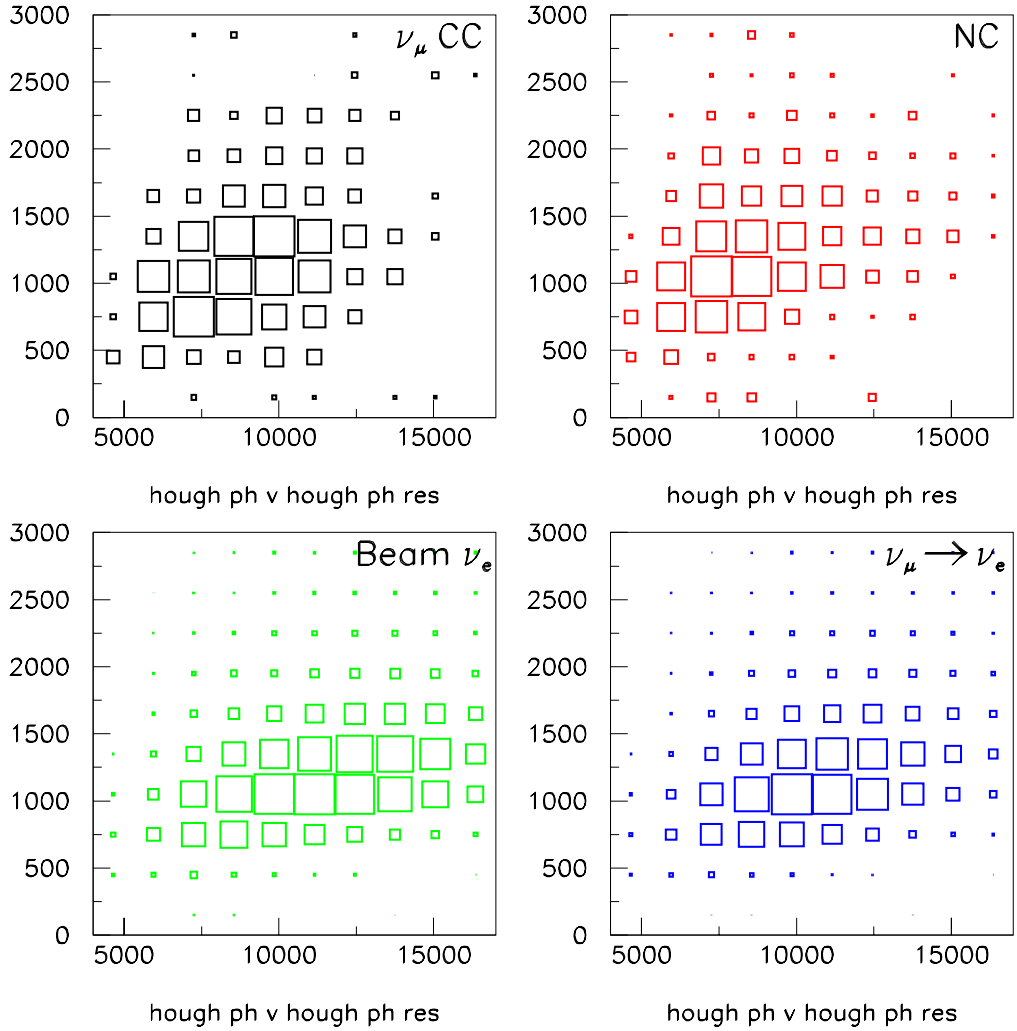

Figure 13 Total pulse height (x) versus pulse height residual (y) distributions from the hits assigned to the Hough track for the four event classes.

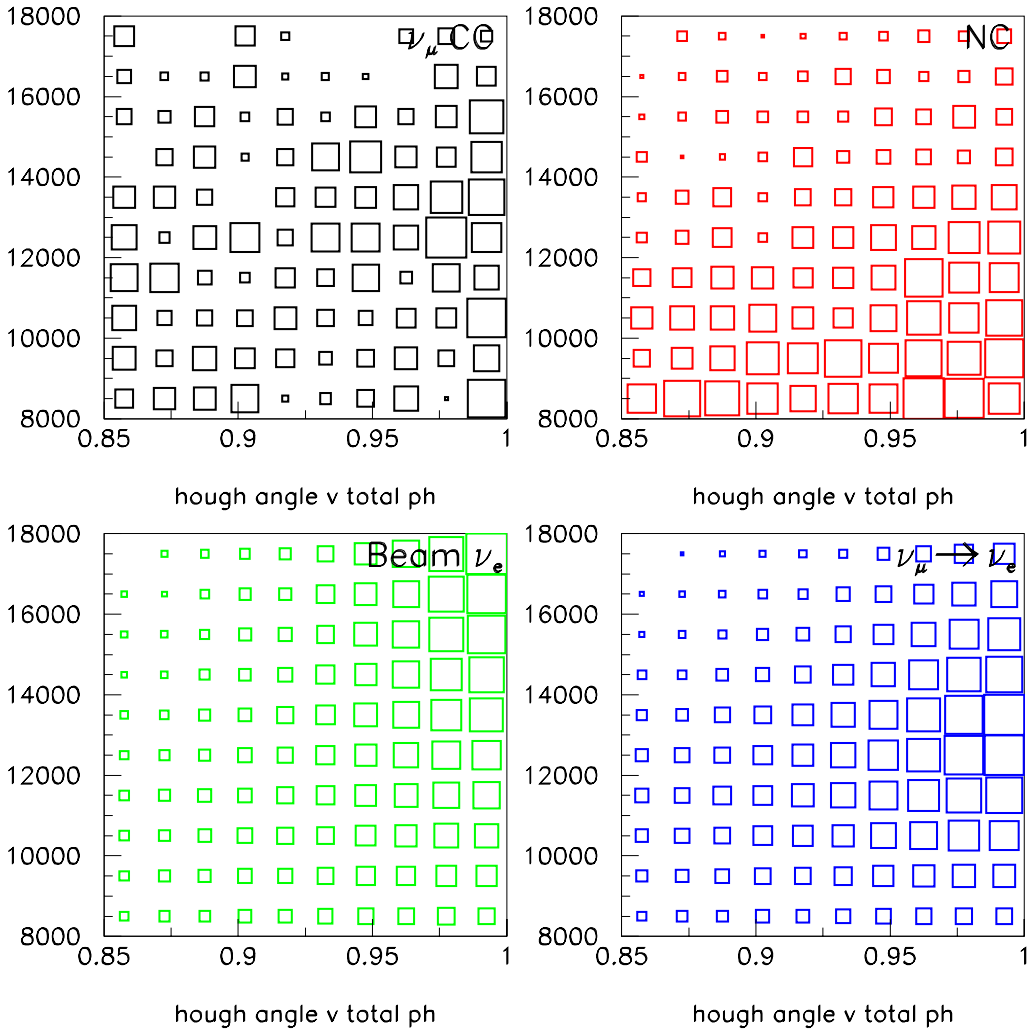

Figure 14 Cosine of the angle between the Hough track and the z axis (x) versus the total pulse height in the event (y)

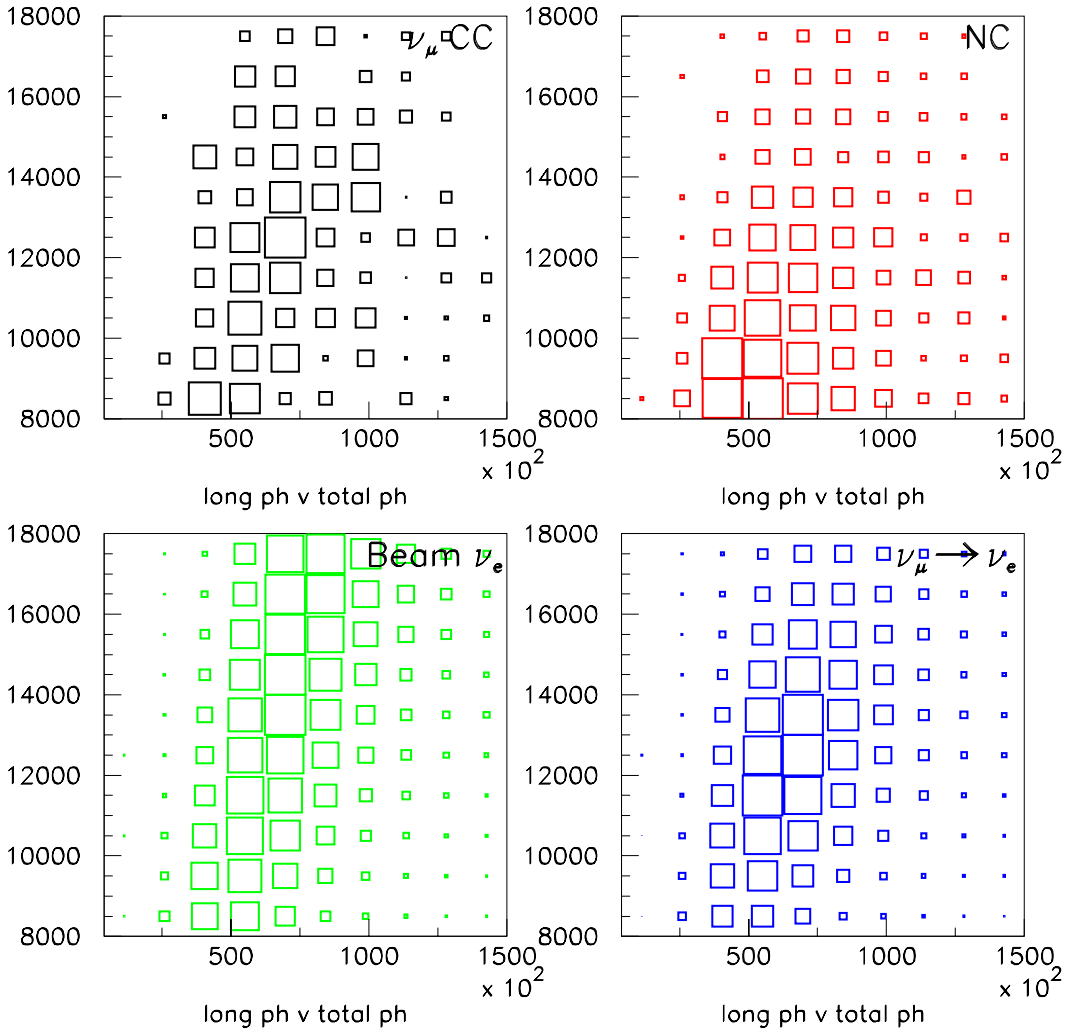

Figure 15 The rms of the pulse height times distance in the z direction (x) versus the total pulse height for hits in the total event (y).

The Log likelihood ratios are shown in Figure 16
There is quite good discrimination between ν_e signal events and neutral current and charged-current backgrounds. There is less separation between ν_e signal events and beam ν_e background; here the only discrimination is that the beam ν_e events tend to be of higher energy than the $\nu_\mu \rightarrow \nu_e$ signal.

The following cuts on the likelihood ratios define the sample of ν_e events in this analysis:

$$\log \boldsymbol{L}_{e/\mu} > -2, \quad \log \boldsymbol{L}_{e/NC} > -2, \quad \log \boldsymbol{L}_{e/ebeam} > -5$$

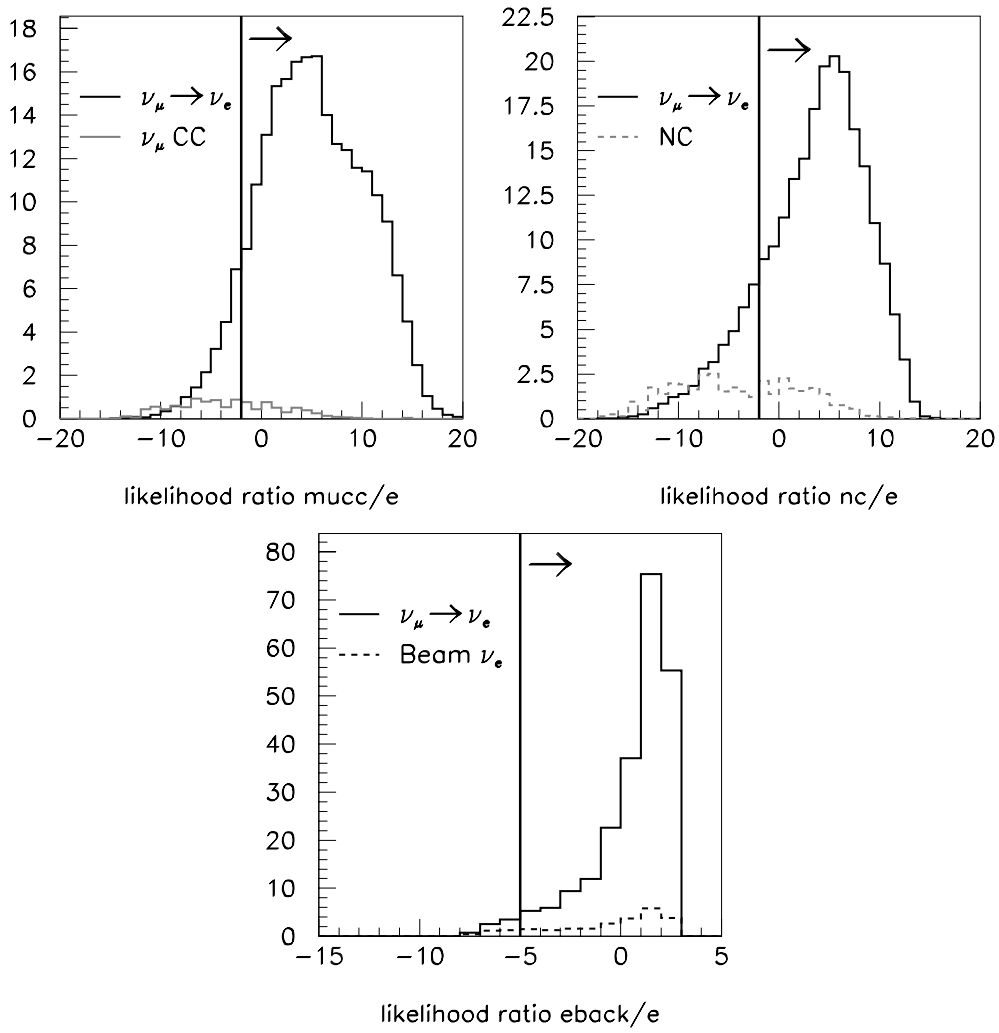

Figure 16 Log likelihood ratio distributions. Top left; log of the ratio of the ν_μ CC to the oscillated ν_e CC likelihood. Top right; log of the ratio of the NC to the oscillated ν_e CC likelihood. Bottom; log of the ratio of the beam ν_e CC to the osciallated ν_e CC likelihood

These cuts on the likelihood ratios were optimized using the first of the two event samples, and were selected in order to maximize the Figure of Merit (FOM). Thedistributions shown here show the result of applying the selection cuts to the second, independent, sample of events. Table 1 shows the breakdown of the event types in this second sample, and the effect of the various cuts on these events.

Defining the figure of merit as the number of $\nu_\mu \rightarrow \nu_e$ signal events divided by the square root of the total number of background (ν_μCC, NC and beam ν_e) events, the following results are obtained:

- signal=178.3±1.4 events, background=33.1±1.0 events
- figure of merit=31.0±0.5
- ν_e efficiency=22.9%

- ν_μ CC rejection=2.85×10^{-4}
- NC rejection=1.64×10^{-3}
- ν_e CC rejection=3.59×10^{-2}

Using these cuts, the background due to mis-identified ν_μCC and NC events is reduced to a level that is below the intrinsic beam ν_e background. It seems difficult to reduce the beam background further, since the only difference between beam ν_e and signal $\nu_\mu \rightarrow \nu_e$ events is the energy distribution, and this is already taken into account by including the total pulse height distributions in the cuts and likelihood analysis.

In order to estimate the influence of the pulse height measurement on the selection we have performed a parallel analysis where all the pulse height weighted quantities are replaced by the number of hits, i.e. all pulse height weighting is set to 1.0. Table 2 shows the numbers obtained after optimization of the FOM using the likelihood and number of hit cuts (only the total pulse height cut in the initial selections involves the pulse height) and Figure 17 shows the log likelihood distributions.

The results are;

- signal=195.6±1.4
- background=44.4±1.2
- figure of merit=29.4±0.5
- signal efficiency=25.1%
- ν_μ CC rejection=3.93×10^{-4}
- NC rejection=2.41×10^{-3}
- ν_e CC rejection=4.49×10^{-2}

It can be seen that the likelihood distribution is broader in the pulse height case, particularly for the NC comparison, and thus the discrimination is better. The pulse height provides about 2 units improvement in the figure of merit.

Cut	ν_μ CC	NC	beam ν_e	$\nu_\mu \rightarrow \nu_e$ signal
Likelihood	4.1	18.4	21.9	195.6
Error	0.5	1.1	0.2	1.4

Table 2: Events remaining after the no pulse height analysis

We have investigated a large number of alternative cuts and composition of the likelihood function in attempts to improve the figure of merit with only marginal success. For example adding both the hit and pulse height quantities to the likelihood function results in an improvement of $\approx$0.3. Adding a further 10 quantities and combinations of quantities actually gave a small reduction in the FOM. The cuts were changed to remove more background before the likelihood analysis but after optimization of the likelihood very similar FOM were obtained. The changes mostly spread out the likelihood function but do not alter the fraction of background that lies under the signal. We conclude that

this is an essentially irreducible background that looks identical to the signal in this detector.

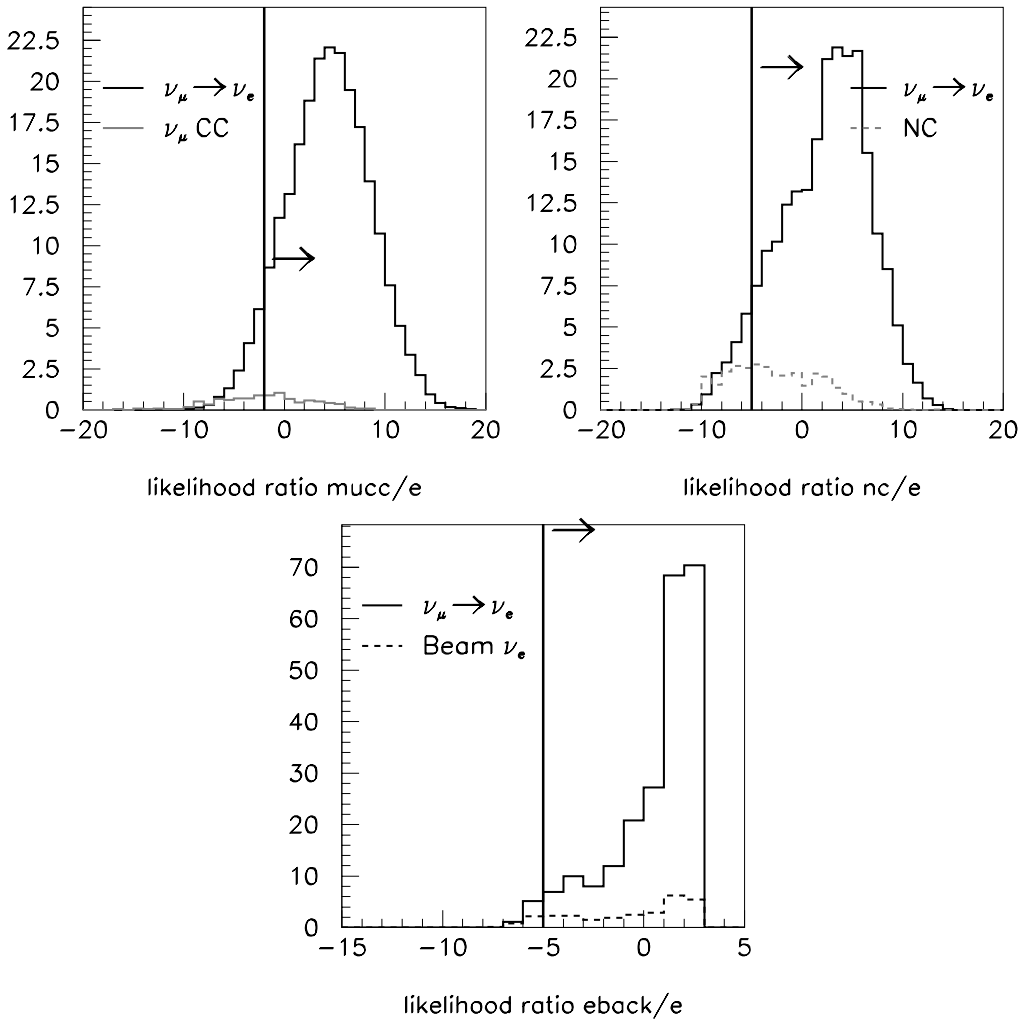

Figure 17 Log likelihood ratio distributions the same as those in Figure 16 except that the pulse height weights in all variables were set to one, that is the pulse height was ignored in the analysis.

Comparison with other analyses

Similar analyses have been performed by Camilleri and Para (OA-note 12) and Yang and Wojcicki using a simulation of an RPC detector. The main differences between the two detectors is that the RPC offers 2-dimensional readout of a single active plane and the scintillator offers pulse height measurements which have some discrimination on the number of particles crossing the plane. The XORY configuration of Camilleri et al

where one view of each plane is ignored should be directly comparable to the no pulse height configuration of this analysis. Their XORY analysis figure of merit is 32.0±1.5, to be compared with 29.4±0.5 of this analysis. These are only marginally in statistical agreement. The main (known) differences between the analyses are;

1. the event generation in this analysis is done throughout the detector, in the XORY analysis events are generated in the center of a small volume of detector and cuts for fiducial volume applied independently later,
2. the fiducial cut is defined by hits outside a fiducial region in this analysis and by a vertex volume in the XORY analysis. An analysis using a vertex cut instead of the hit cut was tried in this analysis with essentially no effect on the FOM,
3. this analysis generated separate samples of NC events and thus has relatively three times the statistics on the NC sample,
4. the overall statistics of this analysis is higher (1.72M ν_μ CC + NC events against 1.17M before removal of duplicated events). Statistics is important in this analysis, after the selections we are left with 146 unweighted events in the ν_μ CC sample and 580 events in the NC sample in the test sample of the no pulse height analysis. Dividing the NC sample by 6 would leave less than 100 events whose statistical fluctuations could be amplified by the weighting,
5. the material between active planes is 0.36 X_0 in this analysis against 0.3X_0 in the XORY analysis.
6. the strip width in this analysis is 4cm compared with 3cm in the XORY analysis
7. events were generated down to 100 MeV in this analysis compared to 1 GeV in the XORY analysis. There are few actual beam events below 1 GeV and cutting out the low energy events made only a small difference to the analysis.

These differences, particularly the strip and sampling frequency differences together with the statistical errors are probably sufficient to account for the small difference in the FOM.

The analysis of Yang et al only studied the 2 view configuration of the RPCs. It is thus difficult to compare with this analysis. They find an FOM of 35.7 which is significantly higher than the 32.9±1.5 of Camilleri et al. and the result of this analysis.

References

1) Roger Rusack, Signals and Noise in the Scintillator Strip detector.
2) L. Camilleri and A. Para, A study of n Off-axis Detector Performance as a Function of Sampling Frequency, Off-Axis-NOTE-SIM-12.
3) T.J.Yang and S. Wojcicki, A study of the dependence of an Off-axis Detector Performance on the strip width and track finding/fitting parameters.